Jurnal Kejuruteraan 37(7) 2025: 3471-3481
https://doi.org/10.17576/jkukm-2025-37(7)-26

Mechanical Performance of Zirconia-Toughened Alumina Composites: The Dual Role of Nitinol as a Toughening and Sintering Aid

Raqibah Najwa Mudzaffar[a], Afifah Mohd. Ali[a*], Zhwan Dilshad Ibrahim Sktani[b,c], Nik Akmar Rejab[d], Hafizah Hanim Mohd Zaki[a], Norshahida Sarifuddin[a], Zuraida Ahmad[a], Ahmad Zahirani Ahmad Azhar[a] & Norazharuddin Shah Abdullah[d]

[a]*Department of Manufacturing and Material Engineering, Kulliyyah of Engineering, International Islamic University Malaysia, Jalan Gombak, 53100 Gombak, Kuala Lumpur, Malaysia*

[b]*Faculty of Engineering, Universiti Teknologi Brunei, Tungku Highway, Gadong, BE1410, Brunei Darussalam*

[c]*Mechanical and Energy Engineering Techniques, Erbil Technical Engineering College, Erbil Polytechnic University, Erbil 44001, Kurdistan-Region, Iraq*

[d]*School of Materials and Mineral Resources Engineering, Engineering Campus, Universiti Sains Malaysia, 14300 Nibong Tebal, Pulau Pinang, Malaysia*

[*]*Corresponding authors: afifahali@iium.edu.my*

Received 26 February 2025, Received in revised form 24 July 2025
Accepted 24 August 2025, Available online 30 October 2025

ABSTRACT

Zirconia-toughened alumina (ZTA) is an advanced ceramic material used in various applications, including cutting inserts, wear parts, and biomedical applications, due to its improved fracture toughness and suitable hardness. However, further improvement of mechanical properties is still a key consideration for expanding its applicability in such demanding applications. Hence, this study examines the effects of nitinol (NiTi) additions (0–5 wt %) on the physical and mechanical properties of ZTA composites. NiTi was incorporated through wet mixing and the samples were sintered at 1600°C, facilitating liquid-phase sintering at 1300°C. At 2 wt% NiTi, optimal densification (4.197 g/cm³), minimal porosity (0.135%), and maximum hardness (1684.15 HV) were achieved, primarily due to microstructural refinement and the Hall-Petch effect. At higher NiTi content (5 wt%), enhanced fracture toughness (5.966 MPa·m$^{1/2}$) was observed, resulting from crack-bridging and stress dissipation enabled by NiTi's ductility and the presence of the retained B2 austenite phase. X-ray diffraction (XRD) analysis confirmed phase stability with no evidence of secondary phase formation. These findings highlight a trade-off between hardness and fracture toughness, demonstrating NiTi's dual role as a sintering aid and toughening agent. The results offer significant potential for tailoring ZTA composites for advanced mechanical applications, particularly in the development of high-performance cutting tools and wear-resistant components.

Keywords: ZTA composites; Nitinol additive; liquid-phase sintering; fracture toughness; hardness

INTRODUCTION

Advanced ceramic materials have become indispensable in high-performance industrial applications due to their exceptional hardness, wear resistance, and thermal stability (Naga et al. 2020). Among these, zirconia-toughened alumina (ZTA) ceramics stand out as a critical material for cutting tools, wear components, and structural parts, combining alumina's inherent hardness with zirconia's transformation-toughening mechanisms (Li et al. 2020; Sktani et al. 2022). Despite these advantages, ZTA ceramics face persistent challenges in balancing fracture toughness with hardness, particularly under extreme mechanical and thermal loads (Manshor et al. 2017; Taib et al. 2019). The brittleness of conventional ZTA often leads to crack

propagation and premature failure, thereby limiting its reliability in demanding applications, such as high-speed machining (Chai et al. 2023; Yan et al. 2023).

Traditional approaches to enhance ZTA's mechanical properties involve incorporating secondary reinforcements like whiskers, fibres, or ductile particles (Niu et al. 2021; Liu et al. 2020). While these additives improve fracture toughness, they often necessitate complex processing techniques such as hot pressing or spark plasma sintering, raising production costs and introduces health hazards (Sktani et al. 2014; Guo et al. 2002). Moreover, such reinforcements can compromise sinterability or introduce porosity, counteracting gains in mechanical performance (Zuo et al. 2018). These limitations underscore the need for innovative strategies to achieve synergistic improvements in both hardness and fracture resistance through microstructural design (Sktani et al. 2019).

Recent advancements have explored the integration of shape-memory alloys (SMAs) into ceramic matrices to address these challenges. Nickel-titanium (NiTi), a prominent SMA, exhibits unique super-elasticity (Chen et al. 2024) and stress-induced phase transformations, enabling energy dissipation during mechanical loading (Guarise et al. 2025). These properties suggest NiTi's potential to enhance fracture toughness in ceramic composites by deflecting cracks, absorbing strain energy, and redistributing stress. Preliminary studies on NiTi-reinforced composites report improved crack resistance and damage tolerance (Li et al. 2013), attributed to the alloy's ability to undergo reversible martensitic transformations under stress (Zhang et al. 2023). However, the incorporation of NiTi into ZTA ceramics remains underexplored, with a limited understanding of how its concentration influences microstructural evolution and mechanical behaviour.

The compatibility of NiTi with ZTA's oxide matrix presents additional complexities. While NiTi's metallic nature may introduce challenges in interfacial bonding and thermal expansion mismatch during sintering, its ductility and energy-absorbing capabilities could counteract ZTA's brittleness. Prior work on metal-ceramic composites highlights the importance of optimising reinforcement distribution and interfacial strength to prevent agglomeration or pore formation (Zheng et al. 2021; Zheng et al. 2021). For the NiTi-ZTA system, achieving a homogeneous dispersion while maintaining phase stability during high-temperature processing is critical to unlocking its toughening potential (Mahmud et al. 2018).

This study investigates the *in-situ* integration of NiTi into ZTA ceramics to engineer a novel composite microstructure. By systematically varying NiTi content (0–5 wt%), the work evaluates its impact on densification, hardness, and fracture resistance. Advanced characterisation techniques, including scanning electron microscopy (SEM) and X-ray diffraction (XRD), are employed to analyse microstructural features, phase composition, and crack propagation mechanisms. The findings aim to establish a foundational framework for designing NiTi-ZTA composites with tailored mechanical properties, bridging the gap between ceramic durability and metallic resilience for next-generation cutting tools and wear-resistant applications.

METHODOLOGY

MATERIAL

The starting raw materials were Al_2O_3 (Martinswerk, 99% purity), yttria-stabilised zirconia (YSZ) (Goodfellow, 5.4% Y_2O_3, ≥96% purity), and nitinol (NiTi, 55.8% Ni–44.2% Ti, Goodfellow). The Al_2O_3/YSZ weight ratio was fixed at 80:20 because it was found to be the optimum ZTA ceramic composite based on a study (Azhar et al. 2009), while NiTi was added in varying concentrations (0–5 wt%) as shown in Table 1.

TABLE 1. Composition of the ZTA added with NiTi

Materials	Code	Al_2O_3 (wt%)	YSZ (wt%)	NiTi (wt%)
ZTA-0wt%NiTi	ZTN0	80.0	20.0	0.0
ZTA-1wt%NiTi	ZTN1	79.2	19.8	1.0
ZTA-2wt%NiTi	ZTN2	78.4	19.6	2.0
ZTA-3wt%NiTi	ZTN3	77.6	19.4	3.0
ZTA-4wt%NiTi	ZTN4	76.8	19.2	4.0
ZTA-5wt%NiTi	ZTN5	76.0	19.0	5.0

PREPARATION OF SAMPLES

Raw powders of Al_2O_3, YSZ, and NiTi were wet-mixed with distilled water and alumina balls (5 mm diameter) in a poly-ethylene bottle using a Lab Roll ball mill (QM-5) at 100 rpm for 24 hours. The resulting slurry was oven-dried at 100°C for 24 hours (Contherm Thermotec 2000), ground into fine powder using an agate mortar, and mixed with 1 ml polyethylene glycol (PEG 400 mol) as a binder. The powder-binder mixture was uniaxially pressed into cylindrical green bodies (13 mm diameter) at 100 MPa for 2 minutes using a hydraulic hand press (Carver). Finally,

the samples were sintered in a Yudian Muffle furnace at the optimum sintering temperature of 1600°C (Sktani et al. 2021) for 1 hour with a heating/cooling rate of 5°C/min to ensure densification and phase stability. The fabricated ZTA ceramics with 0-5 wt% NiTi additives are shown in Figure 1.

FIGURE 1. ZTA samples with 0-5 wt% NiTi additives

CHARACTERISATION

The sintered ZTA-NiTi composites were comprehensively characterised to evaluate their physical, mechanical, and microstructural properties. Linear shrinkage, a critical indicator of dimensional stability during sintering (Mohd et al. 2016), was determined by measuring changes in the diameter and thickness of the samples before and after sintering (Figure 2). The shrinkage percentages were calculated using Equations 1 and 2:

$$\text{Linear Shrinkage (\%)} = \frac{D_0 - D_1}{D_0} \times 100\% \quad (1)$$

$$\text{Linear Shrinkage (\%)} = \frac{T_0 - T_1}{T_0} \times 100\% \quad (2)$$

where D_0 and T_0 are the initial diameter and thickness, and D_1 and T_1 are the post-sintering dimensions.

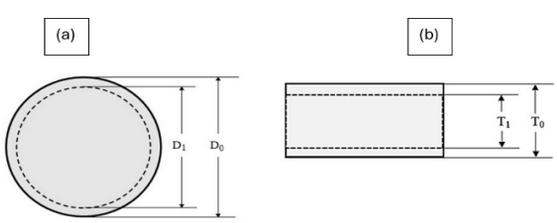

FIGURE 2. Linear shrinkage measurements on the (a) diameter and (b) thickness of the ZTA-NiTi ceramics

Bulk density and porosity, key determinants of mechanical performance, were measured using a GK-300 densimeter. Density was derived from the Archimedes principle, while porosity was calculated through Equation 3:

$$\text{Porosity (\%)} = \frac{W_s - W_d}{W_s - W_a} \times 100\% \quad (3)$$

where W_s, W_d, and W_a represent soaked, dry, and suspended weights, respectively. Five samples per composition were tested to ensure statistical reliability.

Mechanical properties were evaluated through Vickers hardness and fracture toughness tests. Hardness was measured using a diamond indenter (Mitutoyo HV-114) under a 40 kgf load applied for 10 seconds, which was enough to produce a conveniently sized indentation for measurement through a built-in optical microscope without the occurrence of chipping. Fracture toughness (K_{IC}) was assessed using Niihara's indentation method (Equation 4) (Niihara et al. 1982):

$$3K_{IC} = 0.035(Ha^{0.5})\left(\frac{3E}{H}\right)^{0.4}\left(\frac{c}{a}\right)^{-0.5} \quad (4)$$

Here, H is Vickers hardness, a is half the indentation diagonal, c is crack length, and E (Young's modulus) was estimated using the rule of mixtures.

While the indentation fracture (IF) method is widely criticised for its limited correlation with intrinsic fracture toughness (K_{IC}), it remains practical for comparative studies within the same material system (Sktani et al. 2018; Miyazaki et al. 2016).

Microstructural analysis was conducted through Scanning Electron Microscopy (SEM, Model JEOL, JSM 5600) on palladium-coated samples to observe grain morphology, phase distribution, and porosity. The microscope is attached to an Energy-dispersive X-ray spectroscopy (EDS) analysis facility to study the chemical composition of the samples. X-ray diffraction (XRD, Bruker D2 Phaser) with CuKα radiation (30 kV, 10 mA) identified phase compositions across a 2θ range of 20°–80°, with peaks cross-referenced against the ICDD database. The PANalytical X'PERT Highscore Plus software was used to perform the qualitative analysis of XRD profiles.

RESULTS

X-ray diffraction (XRD) analysis in Figure 3 revealed dominant peaks corresponding to α-Al_2O_3 (corundum) and yttria-stabilised zirconia (YSZ) in all ZTA-NiTi samples (0–5 wt% NiTi). No secondary phases or impurities, such as $NiAl_2O_4$ or TiO_2, were detected, confirming NiTi's chemical inertness within the ZTA matrix during sintering at 1600°C.

In the ZTN0 sample (0 wt% NiTi), only Al_2O_3 and YSZ peaks were observed. As NiTi was added, distinct NiTi peaks (B2 austenite phase) emerged in the 2θ range of 40°- 50°, with the most prominent peak at 46°. The intensity of these NiTi peaks increased proportionally with NiTi content, confirming its successful integration into the ZTA matrix.

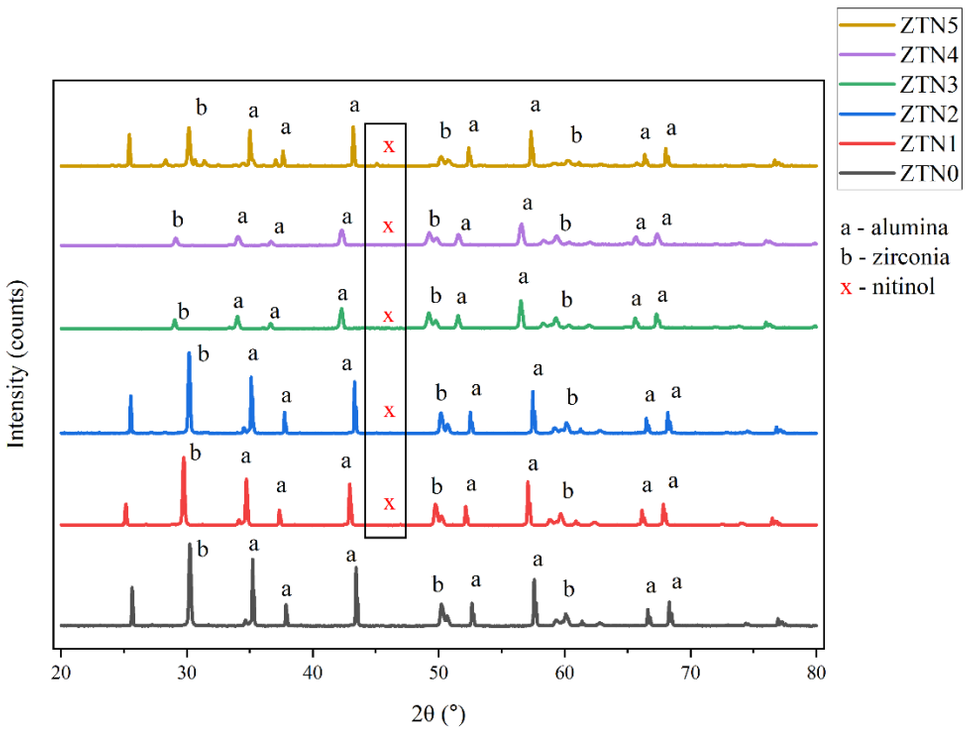

FIGURE 3. XRD pattern of ZTA ceramics with 0 - 5 wt% of NiTi additives

Scanning electron microscopy (SEM) images (Figure 4) illustrated significant microstructural changes with increasing NiTi content. The baseline ZTN0 composite exhibited coarse α-Al_2O_3 grains (grey contrast) and finer YSZ particles (white contrast), with visible interparticle gaps and a porosity of 4.227%. NiTi addition induced progressive grain growth. At 1 wt% NiTi (ZTN1), porosity decreased to 0.311%, resulting in a uniform microstructure. A further decrease in porosity is observed at 2 wt% of NiTi (0.181% at ZTN2), while optimal porosity is achieved at 3 wt% with a value of 0.095%. At this point, the microstructure appears to be more homogeneous and exhibits less visible porosity, with enhanced grain packing. At > 3 wt% NiTi, the agglomeration of NiTi particles becomes apparent, correlating with an increase in porosity upon the addition of 4-5 wt% NiTi (0.91% at ZTN4 and 0.241% at ZTN5).

Energy-dispersive X-ray spectroscopy (EDS) mapping of ZTN2 (Figure 5a) confirmed uniform elemental distribution, with distinct signals for Al, Zr, O, Y, Ni, and Ti. The EDS spectrum (Figure 5b) and elemental composition (Table 2) further validated the presence of Ni and Ti, corroborating XRD results.

TABLE 2. Elemental composition of ZTA-2.0 wt% NiTi

Element	Weight%	Atomic %
O	43.2	4.3
Al	43.2	4.2
Zr	11.1	6.4
Ti	1.4	1.0
Ni	0.6	4.0
Y	0.5	5.0

All samples underwent linear shrinkage in both diameter and thickness during sintering, as shown in Figure 6. The average linear shrinkage for diameter (16.57% for ZTN2) was consistently higher than that for thickness (15.31% for ZTN2), attributed to anisotropic stress distribution during uniaxial compaction. Lower compaction stress along the radial direction (diameter) reduced interparticle contact areas, enhancing shrinkage.

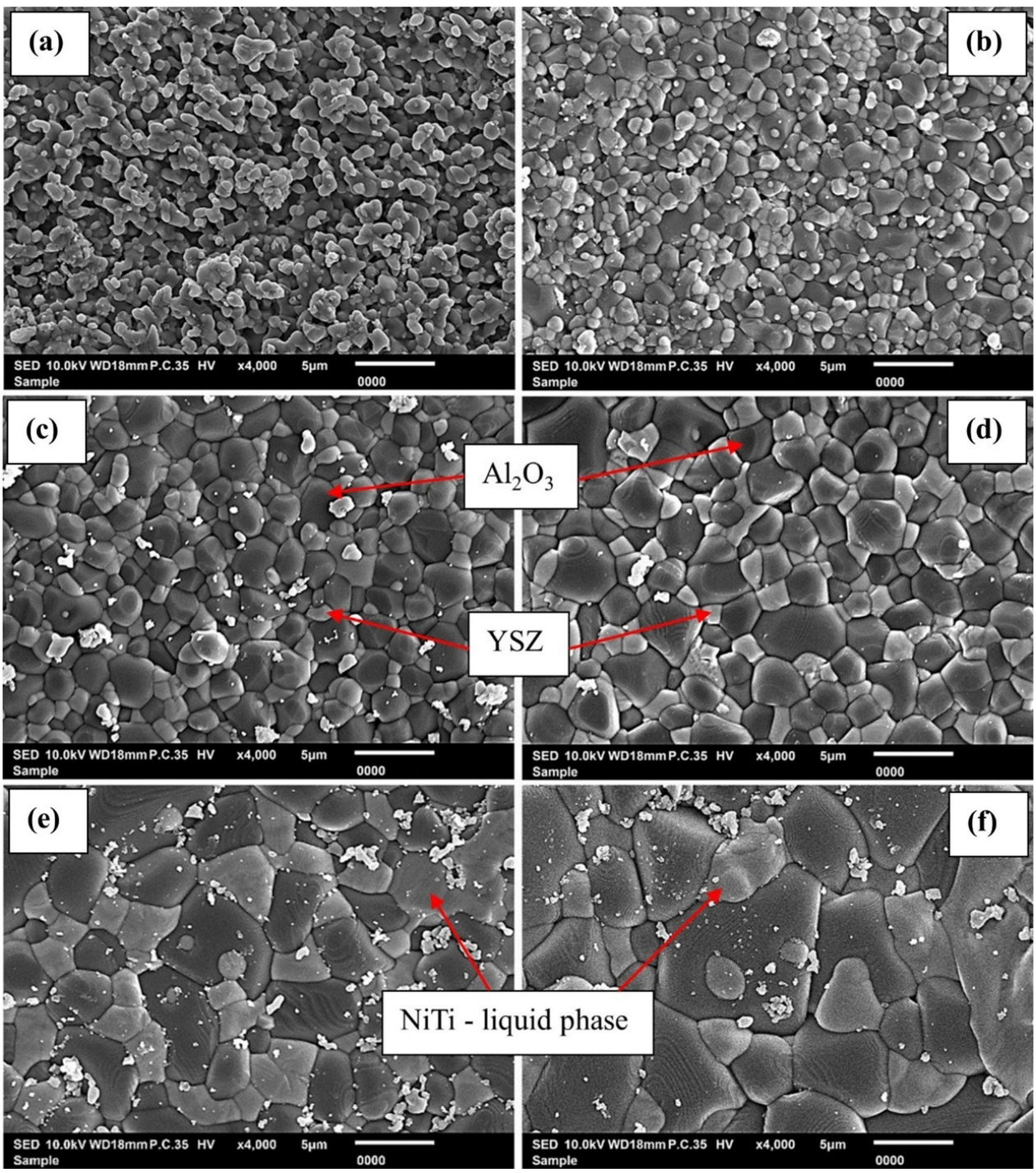

FIGURE 4. Microstructure of ZTA ceramic with (a) 0 wt%, (b) 1 wt%, (c) 2 wt%, (d) 3 wt%, (e) 4 wt%, and (f) 5 wt%, NiTi additives, respectively.

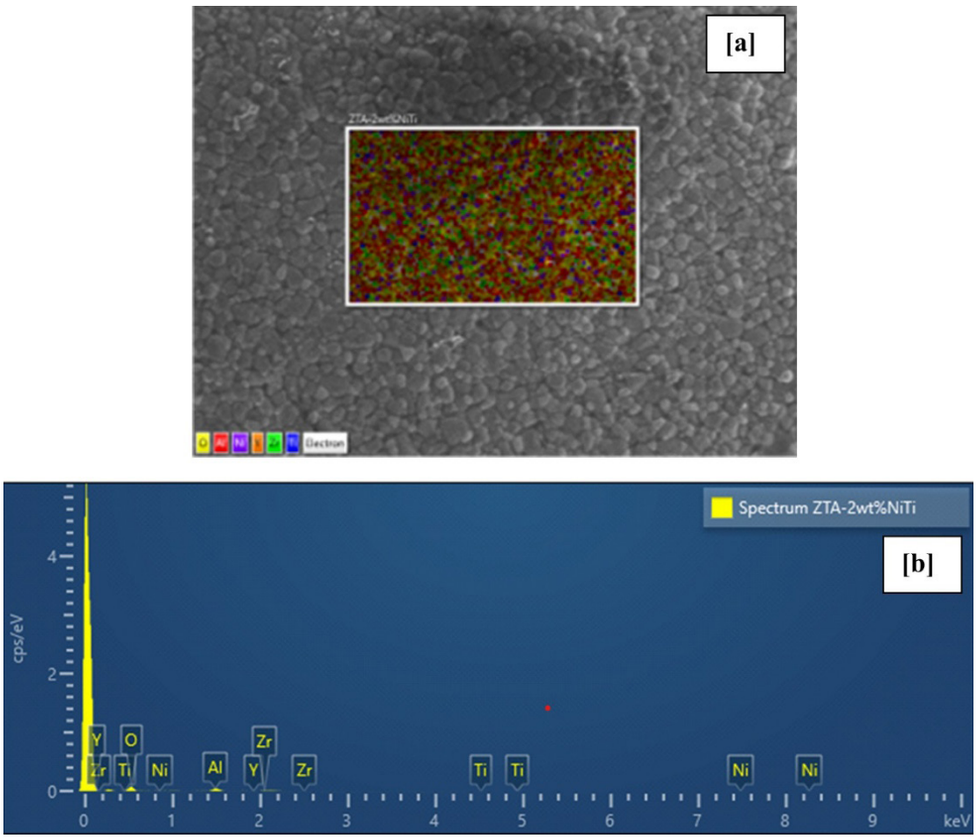

FIGURE 5. (a) EDS mapping of ZTA-2.0 wt% NiTi, (b) Spectrum of ZTA-2.0 wt% NiTi.

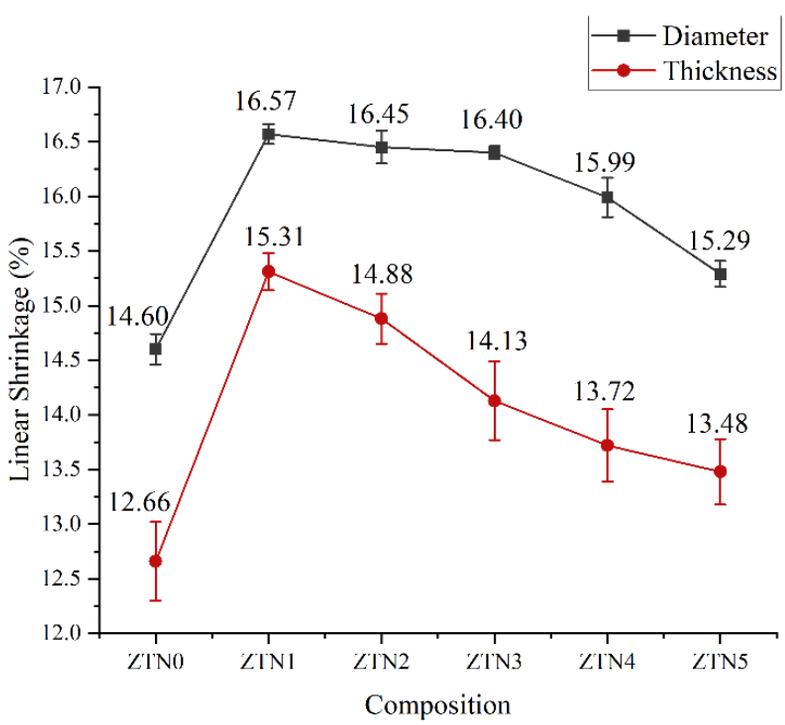

FIGURE 6. Linear shrinkage of ZTA ceramics with 0-5 wt% of NiTi additives.

The shrinkage trend followed a non-linear pattern, with values increasing from ZTN0 (14.60% diameter, 12.66% thickness) to ZTN2 (peak values) before declining in ZTN3–ZTN5. This behaviour reflects the interplay between liquid-phase sintering effects and agglomeration at higher NiTi concentrations.

Bulk density increased progressively with NiTi addition, peaking at 4.197 g/cm³ for ZTN2 as displayed in Figure 7. This represents a 9% improvement over NiTi-free ZTN0 (3.853 g/cm³), driven by liquid-phase sintering mechanisms that filled intergranular voids. Beyond 2 wt% NiTi, density declined to 4.057 g/cm³ (ZTN5), correlating with NiTi agglomeration and porosity reintroduction. Porosity followed an inverse trend, as shown in Figure 7, decreasing from 4.227% (ZTN0) to 0.095% (ZTN3), representing a 98% reduction, before rising to 0.241% (ZTN5). The minimal porosity at ZTN3 confirms the efficacy of NiTi as a pore-filling agent at optimal concentrations.

Vickers hardness peaked at 1684.15 HV for ZTN2 (2 wt% NiTi) before declining to 1251.79 HV at ZTN5 (5 wt% NiTi) as shown in Figure 8. Fracture toughness increased progressively with NiTi content, rising from 4.215 MPa·m$^{1}/_{2}$ (ZTN0) to 5.966 MPa·m$^{1}/_{2}$ (ZTN5) as shown in Figure 8.

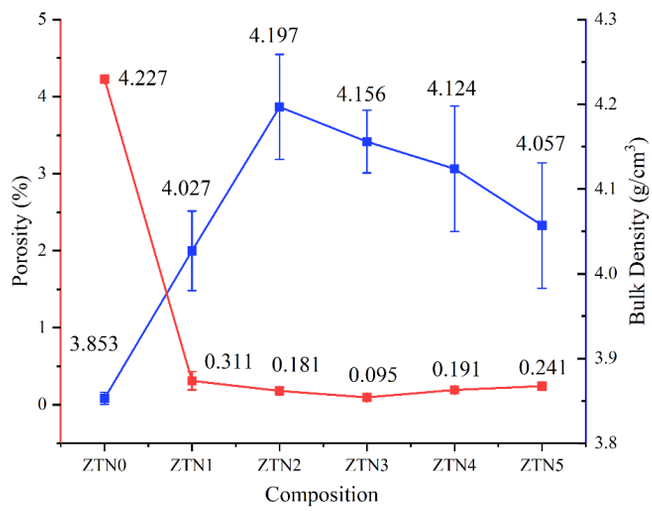

FIGURE 7. Porosity and bulk density of ZTA ceramics with 0-5wt% of NiTi additives

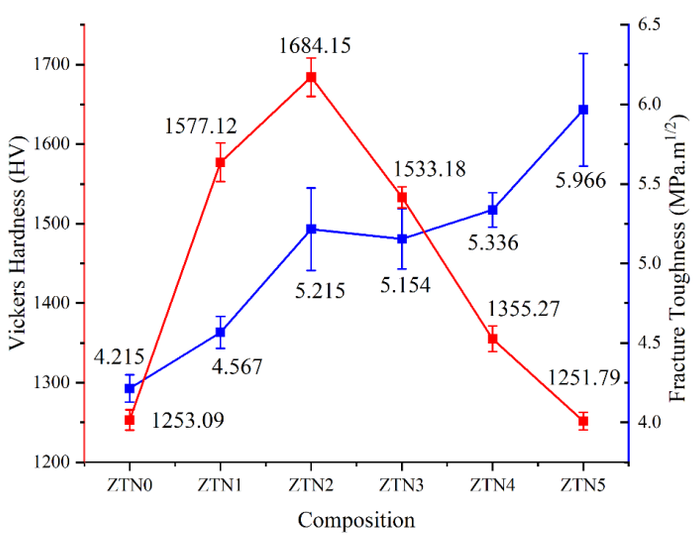

FIGURE 8. Vickers hardness and fracture toughness of ZTA ceramics with 0-5 wt% of NiTi additives

SEM micrographs of fractured surfaces (Figure 9) revealed crack deflection along grain boundaries and crack-bridging mechanisms in NiTi-containing composites. These features were more pronounced at higher NiTi concentrations, explaining the progressive improvement in fracture toughness.

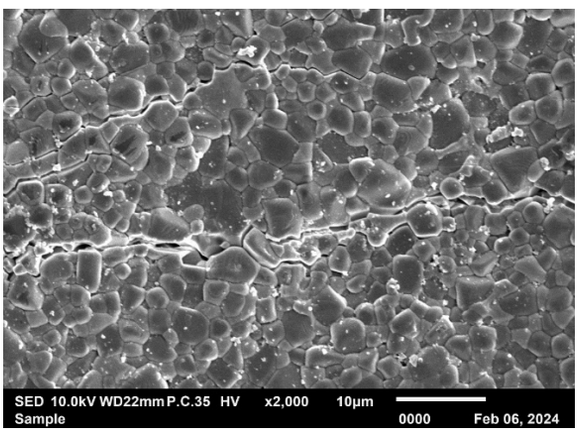

FIGURE 9. SEM micrograph of the fracture path of ZTA-NiTi.

DISCUSSIONS

The integration of nitinol (NiTi) into zirconia-toughened alumina (ZTA) composites has demonstrated significant improvements in both physical and mechanical properties. The findings reveal a complex interplay between NiTi content, microstructural evolution, and mechanical performance, driven by NiTi's dual role as a sintering aid and toughening agent.

The XRD analysis confirmed the chemical inertness of NiTi within the ZTA matrix, as no secondary phases or impurities (e.g., $NiAl_2O_4$ or TiO_2) were detected. This phase stability is critical for maintaining the composites' structural integrity and mechanical performance under high-temperature sintering conditions (Liu et al. 2024). The distinct NiTi peaks (B2 austenite phase) observed in the XRD patterns, emerged in the 2θ range of 40°–50°, with the most prominent peak at 46°, correlated with strong peak of nitinol cubic observed at 41° reported by Khan et al. (2023), demonstrate the successful integration of NiTi into the ZTA matrix without compromising the phase purity of the composite. The absence of additional peaks or phase transformations indicates that NiTi did not react with Al_2O_3 or YSZ, preserving the phase purity of the composite. This phase stability is critical for maintaining the composites' structural integrity and mechanical performance under high-temperature processing conditions (Bakhtiari et al. 2018). The absence of secondary phases from XRD analysis demonstrated the chemical inertness of NiTi within the ZTA matrix, which is critical for preserving mechanical performance by avoiding high-temperature reactions that could weaken the matrix (Liu et al. 2024). This phase stability ensures that microstructural and mechanical changes arise solely from physical mechanisms, such as liquid-phase sintering and crack-bridging effects, rather than chemical interactions. The retention of NiTi's metallic structure enables the exploitation of its unique properties, including stress-induced martensitic transformations, to enhance toughness.

Microstructural evolution plays a crucial role in determining the properties of composites. The baseline ZTA composite (0 wt% NiTi, ZTN0) exhibited a microstructure characterised by coarse α-Al_2O_3 grains (grey contrast) and finer YSZ particles (white contrast), with visible interparticle gaps as shown in Figure 4a and a porosity of 4.227% as shown in Figure 7. The addition of NiTi induced progressive grain growth. This phenomenon is attributed to liquid-phase sintering: NiTi melts at 1300°C (Liu et al. 2017), forming a transient liquid that infiltrates intergranular voids during sintering at 1600°C. The liquid phase enhances mass transfer through capillary forces, facilitating particle rearrangement and dissolution-reprecipitation processes (Ostwald ripening) (Liu et al. 2017). Smaller Al_2O_3 and YSZ particles dissolve into the molten NiTi and reprecipitate onto larger grains, promoting densification and reducing porosity.

At ≤3 wt% NiTi (ZTN3), the liquid phase optimally filled interparticle gaps, achieving minimal porosity (0.095%) as shown in Figure 7 and a homogeneous microstructure as displayed in Figure 4d. The uniform dispersion of NiTi, corroborated by linearly increasing XRD peak intensities (Figure 3), ensured cohesive interfacial bonding between Al_2O_3 and YSZ phases. However, at higher NiTi concentrations (>3 wt%), excessive surface energy drove the agglomeration of metallic NiTi particles (Figures 4e–f). These agglomerates disrupted the ceramic matrix, reintroducing porosity (0.274% at 5 wt% NiTi), as shown in Figure 7, and locally coarsening the grain structures. Despite this, the overall microstructure remained denser than the NiTi-free ZTA, underscoring NiTi's dual role as a sintering aid and pore-filling agent.

The physical properties of ZTA-NiTi composites are governed by the interplay between NiTi's liquid-phase sintering behaviour and its interaction with the Al_2O_3-ZrO_2 matrix, as elucidated by phase stability (Figure 3) and microstructural evolution (Figure 4). During sintering at 1600°C, NiTi transitions to a liquid phase at its melting point (1300°C) (Liu et al. 2017), while Al_2O_3 and ZrO_2 remain solid. This molten NiTi infiltrates intergranular gaps between Al_2O_3 and ZrO_2 particles (Figure 4 b–f), effectively filling voids and reducing porosity through

capillary-driven particle rearrangement. This mechanism aligns with findings by Wu et al. (2021), where SiO_2 additives similarly enhanced densification in Al_2O_3 composites through liquid-phase filling. The efficacy of NiTi is evident in ZTN3 (3 wt% NiTi), which achieved minimal porosity (0.095%; Figure 7) and peak bulk density (4.156 g/cm³; Figure 7), as the liquid phase eliminated >95% of vacancies. In contrast, ZTN0 (0 wt% NiTi) exhibited loosely packed particles with visible gaps (Figure 4a), resulting in higher porosity (4.227%) and lower density (3.853 g/cm³).

However, exceeding 2 wt% NiTi disrupted this optimisation. At higher concentrations, the high surface area-to-volume ratio of Al_2O_3 particles amplified surface energy (Ahangaran & Navarchian, 2020), driving NiTi agglomeration to minimise energy (Fig. 4e–f). This agglomeration, corroborated by SEM analysis (Figure 4), disrupted particle uniformity, reintroducing vacancies and increasing porosity to 0.241% (ZTN5). The inverse relationship between density and porosity beyond 2 wt% NiTi underscores a critical trade-off: while the liquid phase initially enhances packing, excessive NiTi content destabilises the microstructure through kinetic instability. Hence, the interplay between NiTi content and sintering dynamics reveals a critical threshold: ≤2 wt% NiTi optimises densification through liquid-phase redistribution, while higher concentrations prioritise microstructural heterogeneity to improve toughening mechanisms (Liu et al. 2024).

The phase stability of NiTi, evidenced by XRD's absence of secondary phases (Figure 3), ensures that densification arises solely from physical mechanisms (liquid-phase filling) rather than chemical interactions. This inertness is pivotal, as reactive additives could form brittle interphases, compromising mechanical integrity (Liu et al. 2024). The microstructure-property linkage clarifies the threshold behaviour: at ≤2 wt%, NiTi's liquid phase optimises particle rearrangement and pore elimination, achieving near-theoretical density. Beyond this, agglomeration-driven porosity dominates, reflecting competing sintering dynamics.

These findings emphasise NiTi's dualistic role—enhancing densification at low concentrations while introducing defects at higher loadings. The results align with sintering theories, validating NiTi as a tunable additive for ZTA composites. For practical applications, this necessitates a balance: ≤2 wt% NiTi prioritises minimal porosity and high density, whereas higher concentrations may be justified in scenarios where microstructural heterogeneity supports enhanced mechanical resilience.

The mechanical behaviour of ZTA composites, including hardness and fracture toughness, is intrinsically linked to phase stability (Figure 3), microstructural evolution (Figure 4), and densification dynamics (Figure 7), which are governed by NiTi addition. Vickers' hardness exhibited a non-linear dependence on NiTi content, peaking at 1684.15 HV for ZTN2 (2 wt% NiTi) before declining to 1251.79 HV at ZTN5 (5 wt% NiTi) (Figure 8). This trend correlates with porosity (Figure 7) and the fine-grained microstructure at 2 wt% NiTi (Figure 4), which maximises hardness through enhanced grain boundary strengthening (Hall-Petch effect) and reduced defect density. Beyond 2 wt%, agglomeration-induced porosity (0.241% at ZTN5) and grain coarsening weaken load-bearing capacity, diminishing hardness.

In contrast, fracture toughness (K_{IC}) increased progressively with NiTi content, rising from 4.215 $MPa \cdot m^{1/2}$ (ZTN0) to 5.966 $MPa \cdot m^{1/2}$ (ZTN5) (Figure 8). This improvement is attributed to NiTi's dual role as a ductile phase and stress-absorbing agent. At ≤2 wt%, the homogeneous dispersion of NiTi (Figure 4) enhanced interfacial cohesion, while its retained B2 austenite phase (Figure 3) enabled stress-induced martensitic transformations, dissipating strain energy during crack propagation. At higher concentrations (>2 wt%), agglomerated NiTi particles (Fig. 4e–f) formed localised ductile networks that bridged cracks and deflected their paths, as observed in SEM analysis of fractured surfaces, as shown in Figure 9. Despite increased porosity at 5 wt% NiTi, the dominance of these toughening mechanisms outweighed porosity-induced weaknesses. The retained B2 austenite phase of NiTi (Figure 3) enables stress-induced martensitic transformations, which absorb strain energy and enhance crack resistance. However, the fracture toughness gain comes at the cost of reduced hardness, highlighting the inherent trade-off between these properties.

The inverse relationship between hardness and toughness beyond 2 wt% NiTi underscores a microstructurally driven trade-off. Phase stability (Figure 3) ensured NiTi's inertness, preventing brittle interphase formation and preserving the ZTA matrix's integrity. Meanwhile, liquid-phase sintering (Figure 4) facilitated pore elimination at low NiTi levels but introduced agglomeration-driven defects at higher loadings. This duality highlights NiTi's tunable functionality: ≤2 wt% optimises hardness through densification (Figure 7 and Figure 8), while ≥5 wt% priorities toughness through microstructural heterogeneity (Figure 4).

These findings align with composite design principles, where reinforcement distribution and interfacial cohesion dictate mechanical performance. The synergy between NiTi's phase stability (Figure 3), pore-filling capability, and ductile toughening mechanisms (Figure 4) positions NiTi-ZTA as a versatile material system, adaptable to applications demanding either wear resistance (e.g., cutting tools) or crack tolerance (e.g., structural components).

Future work could explore graded architectures to spatially decouple these competing properties, leveraging insights from the phase-microstructure-property linkages in this study.

CONCLUSION

This study demonstrates that the strategic incorporation of nitinol (NiTi) into zirconia-toughened alumina (ZTA) composites enables a tunable balance between hardness and fracture toughness, addressing a longstanding challenge in ceramic materials. At 3 wt% NiTi, the composite achieves optimal densification (4.197 g/cm³), and minimal porosity (0.181%), while the peak hardness (1684.15 HV) at 2 wt% NiTi, driven by liquid-phase sintering and microstructural refinement via the Hall-Petch effect. Conversely, increasing NiTi to 5 wt% enhances fracture toughness (5.966 MPa·m$^{1/2}$) through crack-bridging and stress dissipation mechanisms, facilitated by NiTi's retained B2 austenite phase and ductility, despite a slight rise in porosity (0.241%).

The dual functionality of NiTi—as a sintering aid and toughening agent—underscores its versatility in tailoring ZTA composites for specific applications. For high-wear environments such as cutting tools, **ZTN2 (2 wt% NiTi)** offers superior hardness and wear resistance. In contrast, **ZTN5 (5 wt% NiTi)** is better suited for impact-resistant applications requiring crack tolerance. The absence of secondary phases, confirmed by XRD, ensures phase stability and validates the physical (rather than chemical) basis of these enhancements.

Future research should explore **graded microstructures** to spatially optimize hardness and toughness within a single component, alongside hybrid reinforcement strategies combining NiTi with secondary additives. Such advancements could further bridge the gap between ceramic durability and metallic resilience, paving the way for next-generation composites in extreme mechanical and thermal environments.

This work not only advances the understanding of NiTi-ZTA systems but also provides a scalable framework for designing high-performance ceramics tailored to industrial demands.

ACKNOWLEDGMENT

This work was fully funded by the Ministry of Higher Education (MOHE) through the Fundamental Research Grant Scheme (FRGS/1/2021/TK0/UIAM/02/30). The authors would also like to acknowledge the International Islamic University Malaysia for providing the necessary facilities and support for this research.

DECLARATION OF COMPETING INTEREST

None.

REFERENCES

Ahangaran, F. & Navarchian, A. H. 2020. Recent advances in chemical surface modification of metal oxide nanoparticles with silane coupling agents: A review. *Advances in Colloid and Interface Science* 286: 102298.

Azhar, A. Z. A., Ratnam, M. M. & Ahmad, Z. A. 2009. Effect of Al_2O_3/YSZ microstructures on wear and mechanical properties of cutting inserts. *Journal of Alloys and Compounds* 478: 608–614.

Bakhtiari, S. R., Zhe, J., Shariat, B. S., Yang, H. & Liu, Y. 2018. Role of hydrostatic pressure on the phase stability, the ground state, and the transformation pathways of NiTi alloy. *Scripta Materialia* 151: 57–60.

Chai, J., Zhu, Y., Niu, L., Shen, T., Cui, M. & Wang, Z. 2023. Fabrication and characterization of SiC-ZTA ceramic composites by hot pressing. *Ceramics International* 49: 32799–32807.

Chen, X., Guo, A., Wang, J., Lu, S. & Fu, T. 2024. Temperature dependence of tribological properties in NiTi shape memory alloy: A nanoscratching study. *Tribology International* 197: 109812.

Guarise, A., Bertolini, R., Ghiotti, A. & Bruschi, S. 2025. Wear behaviour of additively manufactured Nitinol cryogenically machined at different cutting speeds. *Tribology International* 204: 110478.

Guo, R., Guo, D., Chen, Y., Yang, Z. & Yuan, Q. 2002. In situ formation of $LaAl_{11}O_{18}$ rodlike particles in ZTA ceramics and effect on the mechanical properties. *Ceramics International* 28: 699–704.

Han, Y., Zhu, J., Yan, H., Lin, C., Zhao, Z., Pan, X. & Wang, S. 2020. Effect of shape-memory alloy NiTi fiber on microstructure and mechanical properties of continuous ceramic Al_2O_3 fiber-reinforced Ti/Al_3Ti metal–intermetallic laminated composite. *Advanced Composites Letters*. 29: 1–9.

Khan, L. A., McCarthy, E., Ahad, I. U. & Brabazon, D. 2023. Analysis of nitinol actuator response under controlled conductive heating regimes. *Results in Engineering* 18: 101047.

Li, S., Zhu, Y., Chai, J., Liu, Y., Niu, L. & Gao, X. 2020. Effects of ZrC content on the microstructure and mechanical property of ZrC/ZTA composites consolidated by hot pressing. *Journal of Alloys and Compounds* 860: 1–8.

Li, Q., Liu, N., Liu, A. & Zhang, H. 2013. Effects of NiTi additions on the microstructure and mechanical properties of Ti(C,N)-based cermets. *International Journal of Refractory Metals and Hard Materials* 40: 43–50.

Liu, L., Chen, X., Li, Q., Chen, S., Chen, Y., Li, J., Li, C. & Luo, L. 2020. Preparation, mechanical properties, and toughening mechanisms of SiCw/SiCp-reinforced zirconia-toughened alumina ceramics. *International Journal of Applied Ceramic Technology* 17: 2083–2093.

Liu, B., Huang, S., Van Humbeeck, J. & Vleugels, J. 2017. Pressureless liquid-phase sintered TiCx_x-NiTi/Ni cermets. *Ceramics International* 43: 9512–9521.

Liu, Y. J., Liu, X. C., Li, K. M., Wu, X., Zhou, S. F., Li, W. & Zhang, W. C. 2024. Fabrication of lightweight 3D interpenetrated NiTi@Mg composite with superior bending properties. *Transactions of Nonferrous Metals Society of China* 34: 3569–3584.

Mahmud, A., Wu, Z., Zhang, J., Liu, Y. & Yang, H. 2018. Surface oxidation of NiTi and its effects on thermal and mechanical properties. *Intermetallics* 103: 52–62.

Manshor, H., Abdullah, E. C., Azhar, A. Z. A., Sing, Y. W. & Ahmad, Z. A. 2017. Microwave sintering of zirconia-toughened alumina (ZTA)-TiO_2-Cr_2O_3 ceramic composite: The effects on microstructure and properties. *Journal of Alloys and Compounds* 722: 458–466.

Miyazaki, H. & Yoshizawa, Y. 2016. Correlation of the indentation fracture resistance measured using high-resolution optics and the fracture toughness obtained by the single edge-notched beam (SEPB) method for typical structural ceramics with various microstructures. *Ceramics International* 42: 7873–7876.

Mohd, A., Shah, N. & Maran, M. 2016. Linear shrinkage of the ZTA ceramic cutting inserts. *Procedia Chemistry* 19: 879–883.

Naga, S. M., El Shaer, M., Awaad, M., & Saleh, M. A. 2020. Effect of soaking time on the properties of $SrAl_{12}O_{19}$/ZTA composites. *Journal of Materials Engineering and Performance* 29: 2920-2925.

Niihara, K., Morena, R. & Hasselman, D. P. H. 1982. Evaluation of KIc of brittle solids by the indentation method with low crack-to-indent ratios. *Journal of Materials Science Letters* 1: 13–16.

Niu, L., Li, S., Zhu, Y., Chai, J., Liu, Y., Shen, T., Jin, P., Zhang, H., Xie, E. & Wang, Z. 2021. Correlation between phase content and mechanical properties of SiCw-ZTA composites sintered by SPS. *Ceramics International* 47: 15059–15066.

Sktani, Z. D. I., Arab, A., Mohamed, J. J. & Ahmad, Z. A. 2022. Effects of additives additions and sintering techniques on the microstructure and mechanical properties of zirconia toughened alumina (ZTA): A review. *International Journal of Refractory Metals and Hard Materials* 106: 105870.

Sktani, Z. D. I., Azhar, A. Z. A., Ratnam, M. M. & Ahmad, Z. A. 2014. The influence of in-situ formation of hibonite on the properties of zirconia toughened alumina (ZTA) composites. *Ceramics International* 40: 6211–6217.

Sktani, Z. D. I., Rejab, N. A. & Ahmad, Z. A. 2019. Tougher and harder zirconia toughened alumina (ZTA) composites through in situ microstructural formation of $LaMgAl_{11}O_{19}$. *International Journal of Refractory Metals and Hard Materials* 79: 60–68.

Sktani, Z. D. I., Rejab, N. A., Ratnam, M. M. & Ahmad, Z. A. 2018. Fabrication of tougher ZTA ceramics with sustainable high hardness through (RSM) optimisation. *International Journal of Refractory Metals and Hard Materials* 74: 78–86.

Sktani, Z. D. I., Rejab, N. A., Rosli, A. F. Z., Arab, A. & Ahmad, Z. A. 2021. Effects of La_2O_3 addition on microstructure development and physical properties of harder ZTA-CeO_2 composites with sustainable high fracture toughness. *Journal of Rare Earths* 39: 844–849.

Taib, M. A. A., Sktani, Z. D. I., Rejab, N. A., Xian, K. C. & Ahmad, Z. A. 2019. Role of addition of La_2O_3 on the phase contents, microstructure and mechanical properties of ZTA-MgO ceramics. *Materials Today: Proceedings* 17: 1086–1092.

Wu, J. M., Li, M., Liu, S. S., Shi, Y. S., Li, C. H. & Wang, W. 2021. Selective laser sintering of porous Al_2O_3-based ceramics using both Al_2O_3 and SiO_2 poly-hollow microspheres as raw materials. *Ceramics International* 47: 15313–15318.

Yan, J., Ma, L. & Wang, J. 2023. Formulation for zirconia toughened alumina (ZTA) reinforced metal matrix composites based on a three-phase concentric inclusion model. *Mechanics of Materials* 181: 104660.

Zhang, Y., Xiao, G., Chen, H., Yi, M., Zhang, J., Chen, Z. & Xu, C. 2023. Effect of NiTi content on the mechanical properties and microstructure of TiB_2–TiN-based composite ceramic material prepared using spark plasma sintering. *Ceramics International* 49: 16690–16699.

Zheng, K., Zhang, Q., Wang, J. & Lu, Y. 2021. Interfacial microstructure and mechanical properties of ZTA/ZTA joints brazed with Ni-Ti filler metal. *Journal of the European Ceramic Society* 41: 2076–2084.

Zheng, K., Zhang, Q., Wang, J. & Lu, Y. 2021. Microstructural characterization and mechanical properties of ZTA/ZTA joint brazed by $Ni_{50}Ti_{50}$ filler metal. *Ceramics International* 47: 2758–2765.

Zuo, F., Meng, F., Lin, D., Yu, J., Wang, H., Xu, S., Guo, W., Cerecedo, C., Valcárcel, V. & Lin, H. 2018. Influence of whisker-aspect-ratio on densification, microstructure and mechanical properties of Al_2O_3 whiskers-reinforced CeO_2-stabilized ZrO_2 composites. *Journal of the European Ceramic Society* 38: 1796–1801.